Short-range cluster spin glass near optimal superconductivity in $BaFe_{2-x}Ni_xAs_2$

Xingye Lu,[1] David W. Tam,[2] Chenglin Zhang,[2] Huiqian Luo,[1] Meng Wang,[1] Rui Zhang,[1] Leland W. Harriger,[3] T. Keller,[4,5] B. Keimer,[4] L.-P. Regnault,[6] Thomas A. Maier,[7] and Pengcheng Dai[2,1,*]

[1]*Beijing National Laboratory for Condensed Matter Physics, Institute of Physics, Chinese Academy of Sciences, Beijing 100190, China*

[2]*Department of Physics and Astronomy, Rice University, Houston, Texas 77005, USA*

[3]*NIST Center for Neutron Research, National Institute of Standards and Technology, Gaithersburg, Maryland 20899, USA*

[4]*Max-Planck-Institut für Festkörperforschung, Heisenbergstrasse 1, D-70569 Stuttgart, Germany*

[5]*Max Planck Society Outstation at the Forschungsneutronenquelle Heinz Maier-Leibnitz (MLZ), D-85747 Garching, Germany*

[6]*SPSMS-MDN, UMR-E CEA/UJF-Grenoble 1, INAC, F-38054 Grenoble, France*

[7]*Center for Nanophase Materials Sciences and Computer Science and Mathematics Division, Oak Ridge National Laboratory, Oak Ridge, Tennessee 37831-6494, USA*

(Received 21 May 2014; revised manuscript received 21 June 2014; published 11 July 2014)

High-temperature superconductivity in iron pnictides occurs when electrons are doped into their antiferromagnetic (AF) parent compounds. In addition to inducing superconductivity, electron doping also changes the static commensurate AF order in the undoped parent compounds into short-range incommensurate AF order near optimal superconductivity. Here we use neutron scattering to demonstrate that the incommensurate AF order in $BaFe_{2-x}Ni_xAs_2$ is not a spin-density wave arising from the itinerant electrons in nested Fermi surfaces, but is consistent with a cluster spin glass in the matrix of the superconducting phase. Therefore, optimal superconductivity in iron pnictides coexists and competes with a mesoscopically separated cluster spin glass phase, much different from the homogeneous coexisting AF and superconducting phases in the underdoped regime.

DOI: 10.1103/PhysRevB.90.024509 PACS number(s): 74.25.Ha, 74.70.−b, 78.70.Nx

I. INTRODUCTION

A complete determination of the structural and magnetic phases in solids forms the basis for a comprehensive understanding of their electronic properties [1–4]. For iron pnictides such as $BaFe_2As_2$, where superconductivity can be induced by electron doping via Co or Ni substitution, extensive transport [5,6] and neutron-diffraction work [7–10] have established the overall structural and magnetic phase diagrams for $BaFe_{2-x}Co_xAs_2$ [11,12] and $BaFe_{2-x}Ni_xAs_2$ [13,14]. In the undoped state, $BaFe_2As_2$ forms a collinear antiferromagnetic (AF) order with moment along the a_o-axis direction of the orthorhombic structure [see left inset in Fig. 1(a)] [4]. Upon electron doping to induce superconductivity, the static ordered moment and the Néel temperature (T_N) of the system decrease gradually with increasing x [7]. While the static AF order is commensurate with the underlying lattice and coexists with superconductivity in the underdoped regime [8–10], it abruptly changes into transversely incommensurate short-range order for x near optimal superconductivity [12–14]. This has been hailed as direct evidence that the static AF order in iron pnictides arises from the formation of a spin-density wave driven by itinerant electrons and Fermi-surface nesting of the electron and hole pockets [12,15], much like the spin-density-wave state of the chromium alloys [16].

If the incommensurate AF order in iron pnictides near optimal superconductivity indeed arises from the itinerant electrons and nested Fermi surfaces, one would expect that its incommensurability δ near the AF ordering wave vector, or $\mathbf{Q} = (1, \pm\delta, 3)$ in the right inset of Fig. 1(a), will increase smoothly with increasing electron doping due to the gradually mismatched electron and hole Fermi surfaces [Figs. 1(b)–1(e)]. Systematic neutron-diffraction experiments on $BaFe_{2-x}Co_xAs_2$ [11,12] and $BaFe_{2-x}Ni_xAs_2$ [13,14] instead reveal a first-order-like commensurate to incommensurate transition with increasing electron doping and a dramatic reduction in ordered moment in the incommensurate phase. Furthermore, recent nuclear magnetic resonance (NMR) data on $BaFe_{2-x}Co_xAs_2$ near optimal superconductivity indicate the presence of inhomogeneous frozen AF domains (termed cluster spin glass) in the matrix of the superconducting phase [17]. If the short-range incommensurate AF order in electron-doped iron pnictides [12,13] is indeed the cluster spin glass phase, it cannot originate from the itinerant electrons in nested Fermi surfaces, but may be a consequence of the disordered localized moments [18,19]. Given the ongoing debate concerning the itinerant [15] or localized [20–22] nature of the antiferromagnetism in iron pnictides [23], it is important to determine the microscopic origin of the incommensurate AF order and its connection with superconductivity [24,25].

For a prototypical spin glass such as the $Cu_{1-y}Mn_y$ alloy, the ordering temperature of the elastic magnetic scattering decreases systematically with increasing instrumental energy resolution used to separate the true elastic component from the inelastic/quasielastic scattering [26]. The magnetic order parameter is then the "Edwards-Anderson" order parameter [18] measured with the spin-relaxation time $\tau \sim \hbar/\Delta E$ (ΔE is the neutron spectrometer energy resolution) below which the spins freeze [26]. By using neutron spectrometers with vastly different energy resolutions ($1\ \mu\text{eV} \leqslant \Delta E \leqslant 1.5\ \text{meV}$), we find that the onset of quasi-static incommensurate AF order in electron-doped $BaFe_{1.908}Ni_{0.092}As_2$ [13,14] decreases from $T_N = 36 \pm 3$ K measured with $\Delta E \sim 1$ meV to $T_N = 30 \pm 2$ K for $\Delta E = 1\ \mu$eV. Furthermore, our polarized neutron-diffraction measurements indicate that the ordered

*pdai@rice.edu

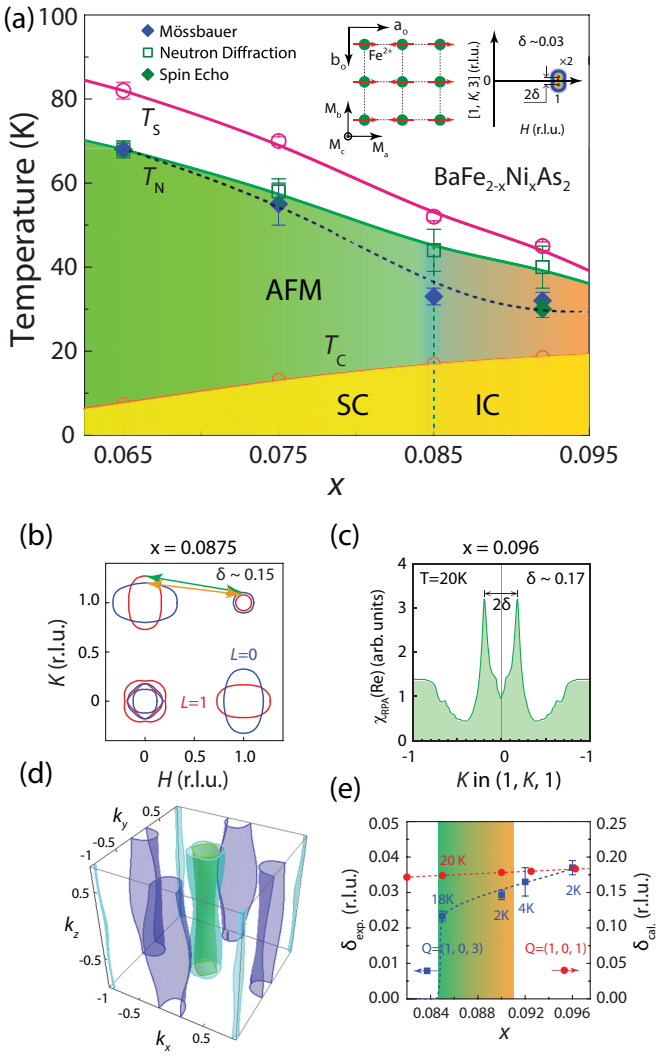

FIG. 1. (Color online) (a) Electronic phase diagram of $BaFe_{2-x}Ni_xAs_2$ in the underdoped regime. The structural (T_s) and magnetic phase transitions (T_N) are taken from Ref. [14]. Filled blue diamonds indicate the measured T_N from Mössbauer measurements of the same samples [41]. The filled green diamond marks the T_N from neutron resonance spin echo (NRSE) measurements. The left panel of the inset shows the spin arrangement of iron in the AF ordered state. M_a, M_b, and M_c are the components of the ordered magnetic moment along the a_o, b_o, and c, respectively. The right panel shows the incommensurate AF peaks in reciprocal space. The scale of the incommensurability is multiplied by a factor of 2 for clarity. (b) Schematic diagram for Fermi surfaces and possible nesting wave vectors for the $x = 0.0875$ sample. The Fermi surfaces at $L = 0$ and 1 are marked as blue and red, respectively. The arrows indicate nesting wave vectors connecting the $L = 0$ and 1 planes. (c) Wave vector dependence of the calculated RPA susceptibility at 20 K for the $x = 0.096$ sample showing transverse incommensurability. (d) Three-dimensional Fermi surfaces of the system in reciprocal space. (e) The electron-doping evolution of the incommensurability from neutron-diffraction experiments (blue squares) [13,14] and RPA calculation (red circles). While the actual electron-doping levels are used in the RPA calculation, x in the figure represents the nominal doping level for easy comparison with experiments. The colored region indicates mixed phases where commensurate and incommensurate AF orders coexist.

moment direction of the incommensurate AF phase is along the longitudinal direction, with no measurable component along the transverse direction. By considering several possibilities for the incommensurate AF order, we conclude that it is a cluster spin glass (or, more precisely, moment amplitude spin glass) in the matrix of the superconducting phase, coexisting and competing with superconductivity [17].

II. THEORETICAL CALCULATION AND EXPERIMENTAL RESULTS

We carried out neutron-scattering experiments on $BaFe_{2-x}Ni_xAs_2$ using SPINS, IN22, and TRISP triple-axis spectrometers at the NIST Center for Neutron Research, Institut Laue-Langevin, and MLZ, respectively. Our samples are grown by the self-flux method [27]. From the inductively coupled plasma (ICP) analysis of the as-grown single crystals, we find that the actual Ni level is 80% of the nominal level x [27]. To allow direct comparison with our earlier measurements, we denote Ni-doping levels as the nominal level. For SPINS measurements, we used the two-axis mode with incident beam energy of $E_i = 5$ meV and triple-axis mode with outgoing neutron energy of $E_f = 2.5$ meV. For the two-axis measurements, there is no analyzer in the exit neutron beam, and neutron energies less than 5 meV can, in principle, be detected, yielding $0 \leqslant \Delta E \leqslant 5$ meV. For the triple-axis measurements, we have $\Delta E \approx 0.1$ meV. For the TRISP measurements, we used $E_f = 14.68$ meV and a 60-mm-thick pyrolytic graphite filter to remove $\lambda/2$ neutrons. The instrument energy resolutions are $\Delta E \approx 1$ meV in the triple-axis mode and $\Delta E \approx 1$ μeV in the neutron resonance spin echo (NRSE) mode [28,29]. Finally, a IN22 triple-axis spectrometer in the polarized neutron-scattering mode was used to determine the moment direction of the incommensurate AF order with instrument setup described in Ref. [30]. We define the wave vector Q at (q_x, q_y, q_z) as $(H,K,L) = (q_x a_o/2\pi, q_y b_o/2\pi, q_z c/2\pi)$ reciprocal lattice units (rlu) using the orthorhombic unit cell suitable for the AF ordered iron pnictide, where $a_o \approx b_o \approx 5.6$ Å and $c = 12.9$ Å. In the undoped state, the commensurate AF order occurs at $\mathbf{Q_{AF}} = (1,0,L)$ with the ordered moment along the a_o direction of the orthorhombic unit cell [left inset in Fig. 1(a)] and $L = 1,3,\ldots$ [4]. For the experiments, we have used single crystals of $BaFe_{2-x}Ni_xAs_2$ with $x = 0.092, 0.096$, where the incommensurate AF order was found along the transverse direction at $\mathbf{Q} = (1,\pm\delta,3)$ [Fig. 1(a)] [13].

Figure 1(a) shows the electronic phase diagram of $BaFe_{2-x}Ni_xAs_2$ as a function of the nominal Ni-doping level x, where the commensurate to incommensurate AF phase transition occurs around $x = 0.085$ in the first-order fashion [13,14]. We first consider if the observed incommensurate AF order can be understood within the itinerant electron Fermi-surface nesting picture [12]. Using a random-phase approximation (RPA) approach [31,32], we calculate the magnetic susceptibility from a tight-binding five-orbital Hubbard-Hund Hamiltonian fitted to the density function theory (DFT) band structure for $BaFe_2As_2$ with a rigid band shift applied to account for electron doping [33]. For the calculation, we used actual Ni doping level determined from the ICP measurements and assumed all the additional Ni

electrons are doped in to the Fe-As planes [27]. This allows us to directly compare the calculated Fermi-surface nesting wave vectors with the neutron-scattering experiments. The interaction matrix in orbital space contains on-site matrix elements for the intra- and interorbital Coulomb repulsions U and U', and for the Hunds-rule coupling and pair-hopping terms J and J'. From the earlier work [32], we know that the RPA calculated Ni-doping evolution of the low-energy spin excitations is in qualitative agreement with the neutron-scattering experiments. To calculate the electron-doping evolution of the incommensurate AF order, we have used the spin rotationally invariant interaction parameters $U = 0.8$, $U' = U/2$, $J = U/4$, and $J' = U/4$ well below the RPA instability threshold. Figure 1(b) shows the Fermi surfaces of $BaFe_{2-x}Ni_xAs_2$ at $x = 0.0875$ and the arrows indicate the nesting wave vectors between the hole pockets at M point and electron pockets. The corresponding incommensurability $\delta = 0.15$ is an average value between $\delta = 0.12$ at $L = 0$ and $\delta = 0.17$ at $L = 1$. Figure 1(c) gives the incommensurability of the $x = 0.096$ sample at $L = 1$. Figure 1(d) shows the full three-dimensional Fermi surfaces used in the calculation. While the calculated evolution of the Fermi surfaces with increasing electron doping is qualitatively consistent with those determined from angle-resolved photoemission experiments [34], comparing the electron-doping dependence of δ from the RPA and experiments [Fig. 1(e)] reveals that the RPA values of δ are about five times larger than the measured values and do not exhibit the commensurate to incommensurate AF order transition near $x = 0.085$ [13]. Although our calculation does not include the electron-lattice coupling effect on the incommensurate AF order, we do not expect that including such an effect will induce first-order-like commensurate to incommensurate AF transition as a function of increasing Ni doping. Therefore, the incommensurate AF order may not originate from a spin-density wave in nested Fermi surfaces.

To test if the incommensurate AF order arises from a cluster spin glass, as suggested from the NMR experiments [17], we carried out neutron-diffraction measurements using SPINS with two-axis and triple-axis modes [35]. Figure 2(a) shows longitudinal scans along the $[H,0,3]$ direction at different temperatures for the $x = 0.092$ sample using the two-axis mode and 60 K scattering data as background. Figure 2(b) shows similar scans using the triple-axis mode with $\Delta E = 0.1$ meV. The temperature dependence of the magnetic order parameters is shown in Fig. 2(c). Since the scattering gradually increases with decreasing temperature, it is difficult to precisely determine the T_N of the system. Nevertheless, we can find its relative changes by using the same criteria for T_N in both measurements. From a simple extrapolation of the low- and high-temperature AF order parameters in Fig. 2(c), we see a clear reduction in the apparent T_N on changing from the two-axis to triple-axis mode. In principle, such a reduction in T_N may result from the temperature differences in the measured critical scattering regimes using different instrumental resolutions, as the critical scattering temperature regime depends sensitively on the spatial and order parameter dimensionality and is generally large in quasi-two-dimensional magnets [36]. However, the spin-spin correlation length should still diverge below T_N [36]. Figure 2(d) shows the temperature dependence of the spin-spin correlation length, obtained by

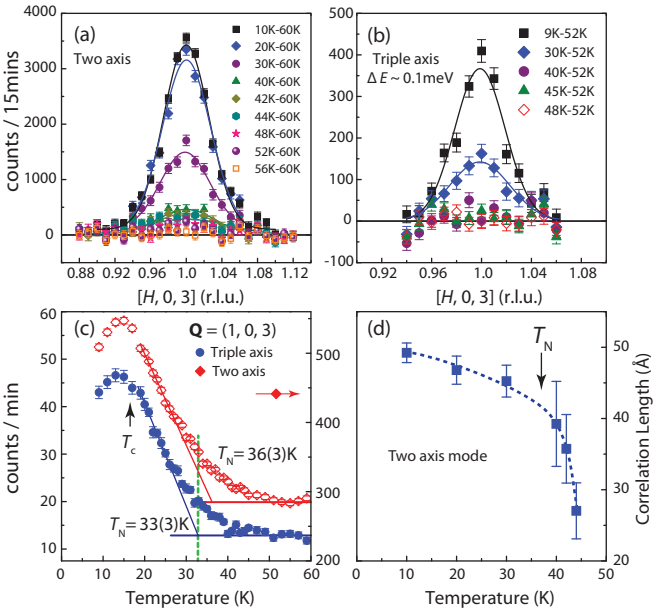

FIG. 2. (Color online) Temperature and wave vector dependence of the incommensurate AF ordering obtained on SPINS using two-axis and triple-axis modes for the $x = 0.092$ sample. (a) Temperature dependence of the longitudinal scans along the $[H,0,3]$ direction using the $T = 60$ K data as background scattering. (b) Identical scans using the triple-axis mode with $\Delta E = 0.1$ meV. The solid lines are Gaussian fits to the data. (c) Comparison of the AF order parameters between the two-axis and triple-axis measurements. The T_N and T_c are marked by the arrow and intersects of the solid lines, respectively. (d) The temperature evolution of the spin-spin correlation length from the two-axis measurements with T_N marked by the arrow. The blue dashed line is a guide to the eye. The vertical error bars indicate the statistical errors of one standard deviation in Figs. 2–4.

Fourier transform of the scattering profiles in Fig. 2(a). Consistent with the earlier work [13], we find that the spin-spin correlation length does not diverge and only reaches to ~50 Å in the low-temperature AF ordered state. These results suggest that the change in the apparent T_N cannot be due to the effect of critical scattering.

Figure 3 summarizes similar measurements on the $x = 0.092$ sample using TRISP, which can operate as a normal thermal triple-axis spectrometer with $\Delta E \approx 1$ meV and a NRSE triple-axis spectrometer with $\Delta E \approx 1$ μeV [28,29]. Figure 3(a) compares the instrumental resolution using the normal and NRSE triple-axis modes. If the AF order is instrumentation resolution limited in the NRSE measurements, we would expect to find the width of the quasielastic scattering Γ to be ~1 μeV. From the temperature dependence of Γ, we see considerable broadening of the quasielastic scattering above 30 K [Fig. 3(b)]. This is consistent with temperature dependence of the magnetic order parameters obtained using the NRSE (red diamonds) modes [Fig. 3(c)]. However, identical measurement using a normal triple axis (blue squares) gives a much higher T_N [Fig. 3(c)]. The large variations in the measured T_N, changing from $T_N = 36 \pm 3$ K at $\Delta E \approx 1$ meV to $T_N = 30 \pm 2$ K at $\Delta E \approx 1$ μeV, means that the spins of the system freeze below 30 K on a time scale

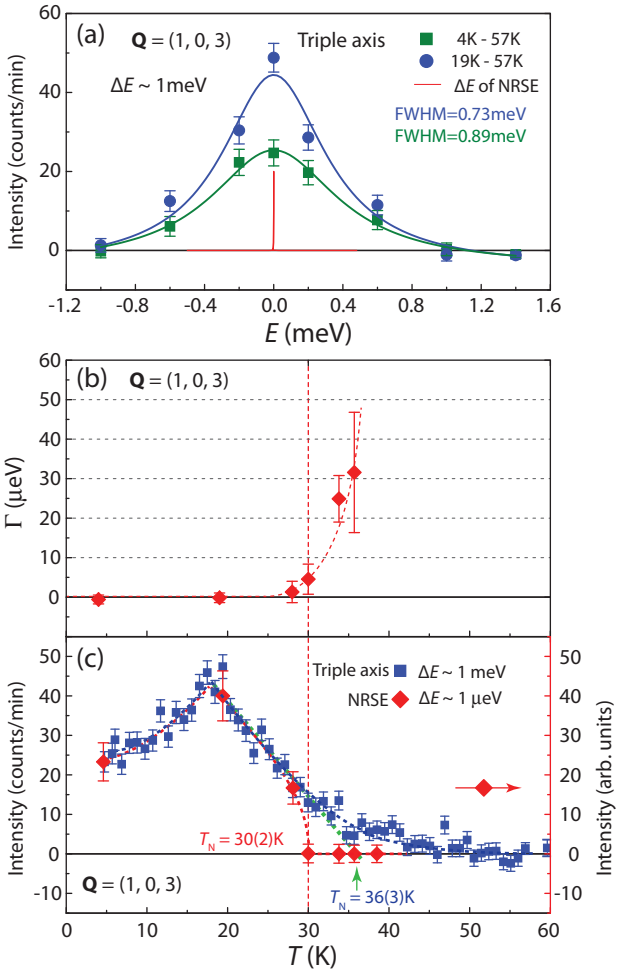

FIG. 3. (Color online) Measurements on the $x = 0.092$ sample using the TRISP triple-axis spectrometer. (a) Temperature difference energy scans measured with the normal triple-axis spectrometer mode at $\mathbf{Q} = (1,0,3)$. They are instrumental resolution limited at $T = 4$, and 19 K using the $T = 57$ K data as background. The red line indicates the effective energy resolution of the NRSE measurement at $\Delta E \approx 1$ μeV. (b) Evolution of the energy width with increasing temperature at $\mathbf{Q} = (1,0,3)$. Γ is the half width at half maximum (HWHM) of scattering function and zero indicates instrumental resolution limited. (c) The magnetic order parameters from the normal triple-axis (blue squares) and NRSE (red diamonds) measurements. The reduction in intensity below ~19 K is due to superconductivity [13]. The T_N from the normal triple axis is estimated by the intersect of two straight lines (green dashed line and black solid line) from the linear extrapolation of the low- and high-temperature data. From NRSE data, one can determine the energy width and integrated intensity of the scattering function $S(Q,E)$. The magnetic order parameter with $\Delta E = 1$ μeV is shown in Fig. 3(c), with T_N marked as a vertical dashed line. The red dashed curves are guides to the eye.

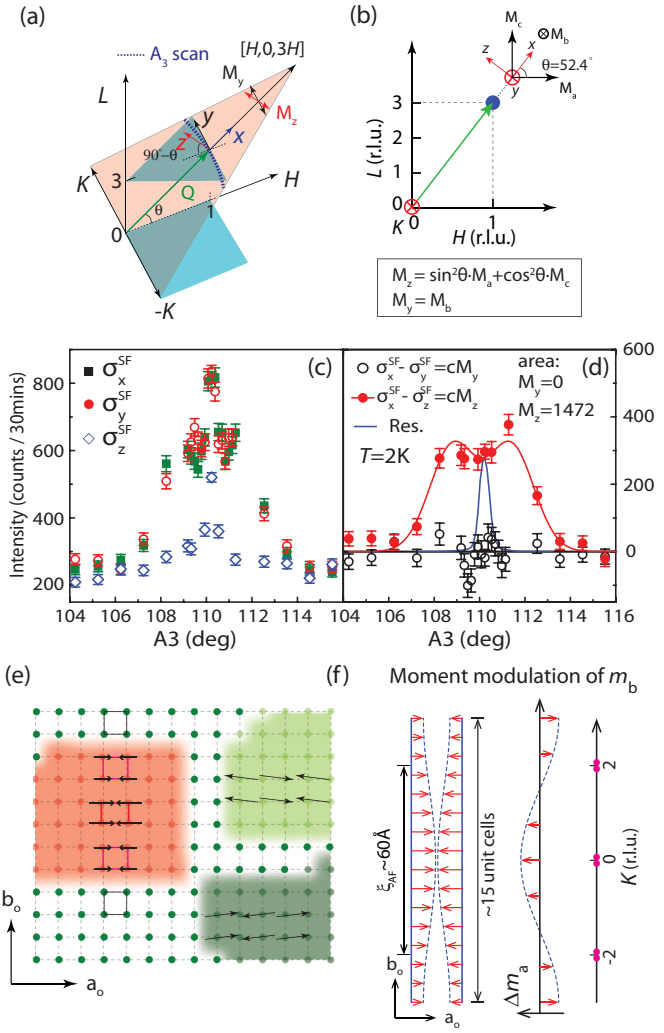

FIG. 4. (Color online) (a) Scattering plane (light pink area) in reciprocal space, $A3$ scan trajectory (blue dashed line), and the neutron polarization directions (x,y,z) with respective to the wave vector $\mathbf{Q}$. (b) The relationship between the neutron polarization directions and magnetic moments along the a_o- (M_a), b_o- (M_b), and c-axis (M_c) directions [30]. M_x, M_y, and M_z are magnetic components along the neutron polarization x, y, and z directions, respectively. (c) Spin-flip scattering cross sections σ_x^{SF}, σ_y^{SF}, and σ_z^{SF} in the $A3$ (rocking curve) scans across $\mathbf{Q} = (1,0,3)$ at $T = 2$ K. (d) $cM_z \sim M(1,0,1/3)$ (solid red line) and $cM_y \sim M_b$ (open circles). The blue solid line shows the instrument resolution obtained using $\lambda/2$. (e) Schematic of the cluster spin glass in the matrix of the superconducting phase. (f) A model of the moment modulating spin-density wave which can give the incommensurate AF order.

of $\tau \sim \hbar/\Delta E \approx 6.6 \times 10^{-10}$ s, similar to the dynamics of a typical spin glass [37].

Another way to establish the origin of the incommensurate AF phase is to determine its ordered moment direction. In an ideal incommensurate spin-density wave, there should be either ordered moment or moment modulations along the incommensurate AF ordering or the b_o-axis direction [16]. To see if this is indeed the case, we used neutron polarization analysis to determine the ordered moment direction in the $x = 0.096$ sample on IN22 [30], which has essentially the same incommensurate AF order as that of the $x = 0.092$ compound. For this experiment, the sample is aligned in the $[H,0,3H]$ and $[0,K,0]$ scattering plane. The incident and outgoing neutron beams are polarized along the $[H,0,3H]$ (x), $[0,K,0]$ (y), and $[-1.3H,0,2.3H]$ $(z$, perpendicular to x and y in the absolute position of Å^{-1}) directions [Fig. 4(a)] [30]. Using neutron spin-flip (SF) scattering cross sections σ_α^{SF},

where $\alpha = x,y,z$, we can extract the magnetic moments M_y and M_z via $cM_y = \sigma_x^{SF} - \sigma_y^{SF}$ and $cM_z = \sigma_x^{SF} - \sigma_z^{SF}$, where $c = (R-1)/(R+1)$ and R ($\approx$15) is the flipping ratio [30]. Since the magnetic moment M_b is equal to M_y and $M_z = M_a \sin^2\theta + M_c \cos^2\theta$ [Fig. 4(b)], we can conclusively determine M_b by measuring σ_x^{SF} and σ_y^{SF}. Figure 4(c) shows rocking curve scans through $\mathbf{Q_{AF}} = (1,0,3)$ for σ_α^{SF}. The estimated $M_b \sim cM_y$ and $M_z \sim c(M_a \sin^2\theta + M_c \cos^2\theta)$ are plotted in Fig. 4(d). To within the errors of our measurements, we find $M_b = 0$, meaning no measurable moments along the b_o-axis direction. Since our data are collected by rotating the crystals at fixed $|\mathbf{Q_{AF}}|$, we are effectively measuring the mosaic distribution of the longitudinally ordered AF phase [Fig. 4(e)].

III. DISCUSSION AND CONCLUSIONS

To understand the microscopic origin of the incommensurate AF phase, we consider two possibilities, as sketched in Figs. 4(e) and 4(f). If the ordered moments of the incommensurate phase are aligned along the longitudinal (a_o-axis) direction, the observed incommensurate scattering may be the mosaic distribution of the commensurate AF phase in the matrix of the superconducting phase, as shown in the green patches of Fig. 4(e). However, a mosaic distribution of the commensurate AF phase should result in a broad peak centered at the AF wave vector, in contrast to the observed transverse incommensurate AF order. Furthermore, such a model cannot explain the magnitude or the doping dependence of the incommensurability. It also does not account for the expected orthorhombic lattice distortion in the incommensurate AF phase. Therefore, this model is unlikely to be a correct description of the observed incommensurate phase. Alternatively, if the incommensurate AF order arises from the moment amplitude modulation along the b_o axis [Fig. 4(f)], an incommensurability of $\delta = 0.03$ would require a spin-spin correlation length of $\sim$15 unit cells or $\sim$80 Å, only slightly larger than the observed $\sim$50 Å correlation length. In principle, an a_o-axis aligned moment of the incommensurate AF order cannot exist in the tetragonal unit cell and must break the C_4 rotational symmetry of the underlying tetragonal crystalline lattice [left inset in Fig. 1(a)] [4]. When incommensurate AF order is initially established below T_N, one can observe clear orthorhombic lattice distortion in x-ray diffraction experiments [14]. When superconductivity sets in below T_c, the orthorhombic lattice distortion and intensity of incommensurate AF peaks are gradually suppressed with decreasing temperature [11–14]. This is consistent with the picture that incommensurate AF order is intimately associated with the orthorhombic lattice distortion. Assuming optimal superconductivity in $BaFe_{2-x}Ni_xAs_2$ prefers a true tetragonal structure, this means that the incommensurate AF phase must be located in the orthorhombic lattice distorted patches in the matrix of the paramagnetic tetragonal phase below T_N [red region in Fig. 4(e)]. Since the lattice distortion from the tetragonal to orthorhombic phase must be gradual, one can imagine a scenario where the incommensurate AF order arises from the moment amplitude modulation along the b_o axis coupled with the tetragonal to orthorhombic structural transition [red patch in Figs. 4(e) and 4(f)]. Below T_c, the volume fraction of the superconducting tetragonal phase grows with decreasing temperature at the expense of the incommensurate AF orthorhombic phase. Although we cannot conclusively determine whether this picture is correct, it is consistent with a cluster spin glass (or amplitude spin glass) and much different from a spin-density wave in nested Fermi surfaces.

The identification that the short-range incommensurate AF phase, a general feature in electron-doped iron pnictides [12,13], is a cluster spin glass challenges the notion that the static AF order in iron pnictides arises from the itinerant electrons in nested Fermi surfaces. Furthermore, since incommensurate AF order competes directly with superconductivity [12,13], one can envision a situation where the cluster spin glass coexists and competes mesoscopically with superconductivity near optimal electron doping. While these results are consistent with μSR measurements on $BaFe_{2-x}Ni_xAs_2$ indicating that the disappearance of static magnetism with increasing x is driven mainly by the loss of the volume fraction of the magnetically ordered region near optimal superconductivity [38], they are different from the underdoped regime where antiferromagnetism and superconductivity coexist homogeneously and compete for the same itinerant electrons [8–10,39,40]. These results are also consistent with ^{57}Fe Mössbauer spectroscopy measurements on the same Ni-doped $BaFe_{2-x}Ni_xAs_2$ [38,41]. With increasing electron doping, the long-range commensurate AF order transforms into a cluster spin glass via the first-order fashion. Upon further doping, the cluster spin glass is replaced by a homogeneous superconducting phase with tetragonal structure. The behavior of the incommensurate AF ordered phase in $BaFe_{2-x}Ni_xAs_2$ is remarkably similar to those of the hole underdoped copper-oxide superconductors such as $La_{1.94}Sr_{0.06}CuO_4$ [42] and $YBa_2Cu_3O_{6+x}$ [43], where the spin freezing temperature depends sensitively on the energy resolution of the probes. Very recently, incommensurate charge ordering in underdoped copper oxides was also found to compete with superconductivity [44,45]. These results, together with the present finding of a cluster spin glass phase in iron pnictides, suggest that the spin and charge ordering competing with superconductivity may be a general phenomenon in the phase diagram of doped high-transition-temperature superconductors.

ACKNOWLEDGMENTS

The work at IOP, CAS is supported by MOST (973 Projects No. 2012CB821400 and No. 2011CBA00110) and NSFC (Projects No. 11374011 and No. 91221303). X.L. and H.L. acknowledge Project No. 2013DB03 supported by NPL, CAEP. We also acknowledge support from the US NSF-DMR-1308603 (Rice University and Oak Ridge National Laboratory) and the Robert A. Welch Foundation Grant No. C-1839 at Rice University.

[1] Y. Kamihara, T. Watanabe, M. Hirano, and H. Hosono, J. Am. Chem. Soc. **130**, 3296 (2008).

[2] C. de la Cruz, Q. Huang, J. W. Lynn, Jiying Li, W. Ratcliff II, J. L. Zarestky, H. A. Mook, G. F. Chen, J. L.

Luo, N. L. Wang, and P. Dai, Nature (London) **453**, 899 (2008).
[3] A. S. Sefat, R. Jin, M. A. McGuire, B. C. Sales, D. J. Singh, and D. Mandrus, Phys. Rev. Lett. **101**, 117004 (2008).
[4] Q. Huang, Y. Qiu, W. Bao, M. A. Green, J. W. Lynn, Y. C. Gasparovic, T. Wu, G. Wu, and X. H. Chen, Phys. Rev. Lett. **101**, 257003 (2008).
[5] P. C. Canfield and S. L. Bud'ko, Annu. Rev. Condens. Matter Phys. **1**, 27 (2010).
[6] J.-H. Chu, J. G. Analytis, C. Kucharczyk, and I. R. Fisher, Phys. Rev. B **79**, 014506 (2009).
[7] C. Lester, J.-H. Chu, J. G. Analytis, S. C. Capelli, A. S. Erickson, C. L. Condron, M. F. Toney, I. R. Fisher, and S. M. Hayden, Phys. Rev. B **79**, 144523 (2009).
[8] D. K. Pratt, W. Tian, A. Kreyssig, J. L. Zarestky, S. Nandi, N. Ni, S. L. Bud'ko, P. C. Canfield, A. I. Goldman, and R. J. McQueeney, Phys. Rev. Lett. **103**, 087001 (2009).
[9] A. D. Christianson, M. D. Lumsden, S. E. Nagler, G. J. MacDougall, M. A. McGuire, A. S. Sefat, R. Jin, B. C. Sales, and D. Mandrus, Phys. Rev. Lett. **103**, 087002 (2009).
[10] M. Wang, H. Luo, M. Wang, S. Chi, J. A. Rodriguez-Rivera, D. Singh, S. Chang, J. W. Lynn, and P. Dai, Phys. Rev. B **83**, 094516 (2011).
[11] S. Nandi, M. G. Kim, A. Kreyssig, R. M. Fernandes, D. K. Pratt, A. Thaler, N. Ni, S. L. Bud'ko, P. C. Canfield, J. Schmalian, R. J. McQueeney, and A. I. Goldman, Phys. Rev. Lett. **104**, 057006 (2010).
[12] D. K. Pratt, M. G. Kim, A. Kreyssig, Y. B. Lee, G. S. Tucker, A. Thaler, W. Tian, J. L. Zarestky, S. L. Bud'ko, P. C. Canfield, B. N. Harmon, A. I. Goldman, and R. J. McQueeney, Phys. Rev. Lett. **106**, 257001 (2011).
[13] H. Q. Luo, R. Zhang, M. Laver, Z. Yamani, M. Wang, X. Y. Lu, M. Y. Wang, Y. C. Chen, S. L. Li, S. Chang, J. W. Lynn, and P. C. Dai, Phys. Rev. Lett. **108**, 247002 (2012).
[14] X. Y. Lu, H. Gretarsson, R. Zhang, X. R. Liu, H. Q. Luo, W. Tian, M. Laver, Z. Yamani, Y.-J. Kim, A. H. Nevidomskyy, Q. Si, and P. C. Dai, Phys. Rev. Lett. **110**, 257001 (2013).
[15] J. Dong, H. J. Zhang, G. Xu, Z. Li, G. Li, W. Z. Hu, D. Wu, G. F. Chen, X. Dai, J. L. Luo, Z. Fang, and N. L. Wang, Europhys. Lett. **83**, 27006 (2008).
[16] E. Fawcett, H. L. Alberts, V. Yu. Galkin, D. R. Noakes, and J. V. Yakhmi, Rev. Mod. Phys. **66**, 25 (1994).
[17] A. P. Dioguardi, J. Crocker, A. C. Shockley, C. H. Lin, K. R. Shirer, D. M. Nisson, M. M. Lawson, N. apRoberts-Warren, P. C. Canfield, S. L. Bud'ko, S. Ran, and N. J. Curro, Phys. Rev. Lett. **111**, 207201 (2013).
[18] S. F. Edwards and P. W. Anderson, J. Phys. F: Met. Phys. **5**, 965 (1975).
[19] J. A. Mydosh, *Spin Glasses: An Experimental Introduction* (CRC, Boca Raton, FL, 1993).
[20] Q. Si and E. Abrahams, Phys. Rev. Lett. **101**, 076401 (2008).
[21] C. Fang, H. Yao, W.-F. Tsai, J. P. Hu, and S. A. Kivelson, Phys. Rev. B **77**, 224509 (2008).
[22] C. Xu, M. Müller, and S. Sachdev, Phys. Rev. B **78**, 020501(R) (2008).
[23] P. C. Dai, J. P. Hu, and E. Dagotto, Nat. Phys. **8**, 709 (2012).
[24] P. J. Hirschfeld, M. M. Korshunov, and I. I. Mazin, Rep. Prog. Phys. **74**, 124508 (2011).
[25] A. V. Chubukov, Annu. Rev. Condens. Matter Phys. **3**, 57 (2012).
[26] A. P. Murani and A. Heidemann, Phys. Rev. Lett. **41**, 1402 (1978).
[27] Y. C. Chen, X. Y. Lu, M. Wang, H. Q. Luo, and S. L. Li, Supercond. Sci. Technol. **24**, 065004 (2011).
[28] T. Keller, K. Habicht, H. Klann, M. Ohl, H. Schneier, and B. Keimer, Appl. Phys. A **74**, s332 (2002).
[29] D. S. Inosov, G. Friemel, J. T. Park, A. C. Walters, Y. Texier, Y. Laplace, J. Bobroff, V. Hinkov, D. L. Sun, Y. Liu, R. Khasanov, K. Sedlak, Ph. Bourges, Y. Sidis, A. Ivanov, C. T. Lin, T. Keller, and B. Keimer, Phys. Rev. B **87**, 224425 (2013).
[30] H. Q. Luo, M. Wang, C. L. Zhang, X. Y. Lu, L.-P. Regnault, R. Zhang, S. L. Li, J. P. Hu, and P. C. Dai, Phys. Rev. Lett. **111**, 107006 (2013).
[31] T. A. Maier, P. J. Hirschfeld, and D. J. Scalapino, Phys. Rev. B **86**, 094514 (2012).
[32] H. Q. Luo, Z. Yamani, Y. C. Chen, X. Y. Lu, M. Wang, S. L. Li, T. A. Maier, S. Danilkin, D. T. Adroja, and P. C. Dai, Phys. Rev. B **86**, 024508 (2012).
[33] S. Graser, A. F. Kemper, T. A. Maier, H.-P. Cheng, P. J. Hirschfeld, and D. J. Scalapino, Phys. Rev. B **81**, 214503 (2010).
[34] P. Richard, T. Sato, K. Nakayama, T. Takahashi, and H. Ding, Rep. Prog. Phys. **74**, 124512 (2011).
[35] C. Zhang, H.-F. Li, Y. Song, Y. Su, G. Tan, T. Netherton, C. Redding, S. V. Carr, O. Sobolev, A. Schneidewind, E. Faulhaber, L. W. Harriger, S. Li, X. Lu, D.-X. Yao, T. Das, A. V. Balatsky, Th. Brückel, J. W. Lynn, and P. C. Dai, Phys. Rev. B **88**, 064504 (2013).
[36] R. J. Birgeneau, H. J. Guggenheim, and G. Shirane, Phys. Rev. B **1**, 2211 (1970).
[37] K. Binder and A. P. Young, Rev. Mod. Phys. **58**, 801 (1986).
[38] C. J. Arguello *et al.* (unpublished).
[39] R. M. Fernandes, D. K. Pratt, W. Tian, J. Zarestky, A. Kreyssig, S. Nandi, M. G. Kim, A. Thaler, Ni Ni, P. C. Canfield, R. J. McQueeney, J. Schmalian, and A. I. Goldman, Phys. Rev. B **81**, 140501(R) (2010).
[40] R. M. Fernandes and J. Schmalian, Phys. Rev. B **82**, 014521 (2010).
[41] J. Munevar, H. Micklitz, J. Agüero, Guotai Tan, Chenglin Zhang, P. C. Dai, and E. Baggio-Saitovitch, Phys. Rev. B **88**, 184514 (2013).
[42] B. J. Sternlieb, G. M. Luke, Y. J. Uemura, T. M. Riseman, J. H. Brewer, P. M. Gehring, K. Yamada, Y. Hidaka, T. Murakami, T. R. Thurston, and R. J. Birgeneau, Phys. Rev. B **41**, 8866 (1990).
[43] D. Haug, V. Hinkov, Y. Sidis, P. Bourges, N. B. Christensen, A. Ivanov, T. Keller, C. T. Lin, and B. Keimer, New J. Phys. **12**, 105006 (2010).
[44] G. Ghiringhelli, M. Le Tacon, M. Minola, S. Blanco-Canosa, C. Mazzoli, N. B. Brookes, G. M. De Luca, A. Frano, D. G. Hawthorn, F. He, T. Loew, M. Moretti Sala, D. C. Peets, M. Salluzzo, E. Schierle, R. Sutarto, G. A. Sawatzky, E. Weschke, B. Keimer, and L. Braicovich, Science **337**, 821 (2012).
[45] M. Le Tacon, A. Bosak, S. M. Souliou, G. Dellea, T. Loew, R. Heid, K-P. Bohnen, G. Ghiringhelli, M. Krisch, and B. Keimer, Nat. Phys. **10**, 52 (2014).